JAERI-M
91-124

CONCEPTUAL DESIGN OF SC MAGNET SYSTEM FOR ITER (V)

— MATERIAL —

August 1991

Hideo NAKAJIMA, Masataka NISHI, Shigenori EGUSA, Kiyoshi YOSHIDA
Hiroshi TSUJI, Tadao SEGUCHI, Miyuki HAGIWARA
M. A. KIRK* and R. C. BIRTCHER*

日本原子力研究所
Japan Atomic Energy Research Institute

JAERI-Mレポートは，日本原子力研究所が不定期に公刊している研究報告書です。
入手の問合わせは，日本原子力研究所技術情報部情報資料課（〒319-11茨城県那珂郡東海村）あて，お申しこしください。なお，このほかに財団法人原子力弘済会資料センター（〒319-11 茨城県那珂郡東海村日本原子力研究所内）で複写による実費頒布をおこなっております。

JAERI-M reports are issued irregularly.
Inquiries about availability of the reports should be addressed to Information Division, Department of Technical Information, Japan Atomic Energy Research Institute, Tokai-mura, Naka-gun, Ibaraki-ken 319-11, Japan.

編集兼発行　日本原子力研究所
印　　刷　㈱原子力資料サービス

JAERI-M 91-124

Conceptual Design of SC Magnet System for ITER (V)
- Material -

Hideo NAKAJIMA, Masataka NISHI, Shigenori EGUSA[+]
Kiyoshi YOSHIDA, Hiroshi TSUJI, Tadao SEGUCHI[+]
Miyuki HAGIWARA[+], M.A. KIRK[*] and R.C. BIRTCHER[*]

Department of Fusion Engineering Research
Naka Fusion Research Establishment
Japan Atomic Energy Research Institute
Naka-machi, Naka-gun, Ibaraki-ken

(Received July 8, 1991)

Japan Atomic Energy Research Institute (JAERI) has been developing a superconducting magnet system for a fusion reactor. One of the key items in developing the superconducting magnets is material development and evaluation. The data of superconducting materials, structural alloys, and non-metallic materials are generated to establish a material data base at JAERI.

This report is prepared to provide available data generated by JAERI to designers of superconducting magnets throughout the world. The following review papers written for the International Thermonuclear Experimental Reactor (ITER) report on conceptual design of magnet system are combined here.

I. Superconducting Material Data
II. Mechanical Properties of the Japanese Cryogenic Steels (JCS) at Cryogenic Temperature
III. Review of Radiation Degradation Studies at JAERI on Composite Organic Insulators Used in Fusion Magnets

---

+ Department of Material Development, Takasaki Radiation Chemistry Research Establishment
* Argonne National Laboratory

Keywords: ITER, Superconducting Magnet, Multifilamentary $(NbTi)_3Sn$, Critical Current Density, Mechanical Properties, Austenitic Stainless Steel, Cryogenic Testing, Radiation Degradation, Composite Organic Insulator

JAERI－M 91－124

ITER用超電導マグネット・システム概念設計（V）
－材料データ－

日本原子力研究所那珂研究所核融合工学部
中嶋 秀夫・西 正孝・江草 茂則[+]・吉田 清
辻 博史・瀬口 忠男[+]・萩原 幸[+]・M.A.KIRK[*]
R.C. BIRTCHER[*]

（1991年7月8日受理）

日本原子力研究所（原研）は，核融合炉用超電導マグネット・システムの開発を行っている。超電導マグネットを開発する上での重要項目の一つに材料開発と材料評価が挙げられ，原研ではこれまでに，材料のデータ・ベース確立を目指して，超電導材料の超電導特性に関するデータ，金属構造材料及び非金属構造材料の機械的特性に関するデータを収集してきた。

本レポートは，原研で得られた貴重なデータを全世界の超電導マグネットの設計者が利用できることを目的として準備されたものであり，ITERのマグネット・システムの概念設計書の一部として書かれた，以下の三つの内容を持つ解説を合わせたものである。

Ⅰ．超電導材料特性データ
Ⅱ．金属構造材料の機械的特性データ
Ⅲ．有機複合絶縁材料の照射劣下特性データ

那珂研究所：〒311－01 茨城県那珂郡那珂町大字向山801－1
＋ 高崎研究所材料開発部
＊ アルゴンヌ国立研究所

Contents

目　　次

PREFACE

All of technical design reports from Japanese contributors to ITER magnet design are listed below:

JAERI-M 91-120
CONCEPTUAL DESIGN OF SC MAGNET SYSTEM FOR ITER (I)
- OVERVIEW -

(1) Design Basis
(2) Toroidal Field Coils
(3) Central Solenoid Coils
(4) Outer Ring Coils
(5) Mechanical Design Guideline

JAERI-M 91-121
CONCEPTUAL DESIGN OF SC MAGNET SYSTEM FOR ITER (II)
- STRESS ANALYSIS -

(1) Toroidal Field Coils at End of Burn
(2) Toroidal Field Coils at Fault Conditions
(3) Center Solenoid Coils
(4) PF Coil Support Structure and Outer Ring Coil
(5) Winding Rigidity Analysis

JAERI-M 91-122
CONCEPTUAL DESIGN OF SC MAGNET SYSTEM FOR ITER (III)
- AC LOSS -

(1) Analysis and Measurement of AC Losses in Large Superconducting Coil
(2) AC Loss Analysis
(3) AC Loss in Cryogenic Structure

JAERI-M 91-123
CONCEPTUAL DESIGN OF SC MAGNET SYSTEM FOR ITER (IV)
- POWER SUPPLY AND CRYOGENIC SYSTEM -

(1) Power Supply System for Magnet System
(2) Fault Analysis of TF Power Supply System
(3) Cryogenic System

JAERI-M 91-124

CONCEPTUAL DESIGN OF SC MAGNET SYSTEM FOR ITER (V)

- MATERIAL -

(1) Superconducting Material

(2) Steels

(3) Insulator

JAERI-M 91-125

CONCEPTUAL DESIGN OF SC MAGNET SYSTEM FOR ITER (VI)

- R&D PROPOSALS -

(1) Requirements of Scalable Model Coil Test

(2) TF Scalable Model Coil

I. Superconducting Material Data

M.Nishi

Superconducting Magnet Laboratory
Japan Atomic Energy Research Institute

1. INTRODUCTION

There are many superconducting materials. Among them, multifilamentary $(NbTi)_3Sn$ wire is the best choice for high-field large superconducting coils at present. Major reasons are its good high-field performance, its confirmed reliability as the wire and the established industrial manufacturing processes. Of course, there are some materials, such as Nb_3Al, which are expected to exceed $(NbTi)_3Sn$ in the future, but their reliable manufacturing process as the wire have not yet established industrially. In this report, the critical current density of recent $(NbTi)_3Sn$ superconducting wire is presented briefly.

2. MANUFACTURING PROCESSES OF MULTIFILAMENTARY $(NbTi)_3Sn$

There are many manufacturing processes of multi-filamentary $(NbTi)_3Sn$ superconductor as follows:

* Bronze process
* Internal tin diffusion process
* Niobium tube process
* Jelly-roll process
* External tin diffusion process
* In situ process
* Powder metallurgy process

  etc.

Each process and the wire manufactured with it have advantages and disadvantages, therefore, we cannot choose one as the best

in general. As the typical processes, we select three of them and explain briefly.

2.1 Bronze process

The bronze processed $(NbTi)_3Sn$ is used widely and its manufacturing process is well established. As shown in Fig.1(a), the $(NbTi)_3Sn$ is formed around the niobium filaments arranged in bronze after the diffusion reaction. The bronze of this process can contain tin only around 10 % for the cold drawing, and moreover, a few times of annealing is necessary during drawing process. Because large amount of bronze remains around the $(NbTi)_3Sn$ filaments after reaction, the critical current density per non-copper area, where bronze is involved, becomes much lower than that per $(NbTi)_3Sn$ itself. However, the superconductor with low AC-losses and with high mechanical strength can get easily by this process.

2.2 Internal tin diffusion processed $(NbTi)_3Sn$

In the internal tin diffusion process, the $(NbTi)_3Sn$ is formed with niobium filaments arranged in copper and with tin arranged in the center of the filament area as shown in Fig.1(b). The annealing during drawing is unnecessary, and the bronze fraction in the conductor after reaction can be much lower than that of the bronze processed one. Therefore, present capacity of this type of superconductor is in the same level as that of the bronze processed one, however, it has higher potential capacity.

2.3 Niobium tube processed $(NbTi)_3Sn$

The superconductor manufactured with this process has very high critical current capacity. In this process, the $(NbTi)_3Sn$ is formed on the inner wall of the niobium tube, in which tin core and copper are arranged before reaction as shown in Fig.1(c). The annealing during drawing is also unnecessary and the tin contents in the niobium tube can raise

near 100 %. Major disadvantage of this type of superconductor is its rather high AC losses, because its filament size is larger than those of other types and the filaments are located in copper instead of bronze.

3. CRITICAL CURRENT DENSITY OF $(NbTi)_3Sn$

Figure 2 shows the highest critical current density curve at 4.2 K of the bronze processed $(NbTi)_3Sn$[1], that of the internal tin diffusion processed one[2] and that of the niobium tube processed one[3] published. The current density data per non-copper area of the superconducting wire actually in the coil operated at 4.2 K are also shown in the same figure. As shown in Table 1, some of these points do not indicate the limit of the wire, the real limit of the wire in use can be recognized by these data.

From the curve in Fig.2, the bronze processed $(NbTi)_3Sn$ and the internal tin processed one can have the critical current density of around 700 A/mm2 at 12 T and 600 A/mm2 at 13 T. With the niobium tube processed $(NbTi)_3Sn$, the critical current density of around 1.9 kA/mm2 at 12 T and 1.5 kA/mm2 at 13 T can be expected. These data show the potential capacity of wires, and therefore, at the coil designing, it should be taken the current density at least 0.7 times lower than the champion data mentioned above or should be taken the data measured with the wire industrially well-established.

4. FUTURE PROSPECT

The present current density data of the $(NbTi)_3Sn$ wire were summarized. The capacity of the $(NbTi)_3Sn$ wire is still improved day by day, and other materials are being developed actively. Therefore, the coil designer will have to refer completely new figure in place of Fig.2 a few years hence.

REFERENCES

1. K. Kamata, H. Moriai, N. Tada, K. Watanabe, A. Nagata, K. Noto, "High-Field Superconducting Critical Values of Titanium Bronze Multifilamentary Nb_3Sn Conductors", IEEE Trans. on Mag., Vol. MAG-23, No.2, 1987, pp.637-640
2. S. Miyashita, K. Yoshizaki, Y. Hashimoto, K. Itoh, K. Tachikawa, "The Structure and Superconducting Properties of Multifilamentry Nb_3Sn Wires prepared by Internal Sn Diffusion Process using Sn-Ti Cores", Adv. in Cryo. Eng. Materials, Vol.32, 1986, pp.995-1002
3. H. Shiraki, S. Nakayama, M. Tanaka, S. Murase, N. Aoki, M. Ichihara, K. Watanabe, K. Noto, Y. Muto, "High-Field Superconducting Properties of Ti Doped Nb_3Sn Conductor by the Nb Tube Method", MRS Int'l. Mtg. on Adv. Mats., Vol.6, 1989, pp.43-48

Table 1 List of superconducting magnets shown in Fig.2

No.	Transport Current [A]	Winding Inner Diameter [mm]	Note
1	330	37.5	No quench
2	158	34	
3	330	79.2	Quench except for Ic
4	531	36.6	reach Ic
5	478	46	reach Ic
6	232	28	Quench except for Ic
7	~575	72	No quench
8	155	50	reach Ic
9	70	38	Quench except for Ic
10	330	110	No quench
11	144	130	Quench except for Ic
12	850	40	No quench
13	800	91	No quench
14	1180	190	No quench
15	~220	60	
16	469	58.4	
17	1327	260	No quench
18	804	149.3	Quench except for Ic
19	1327	330	No quench

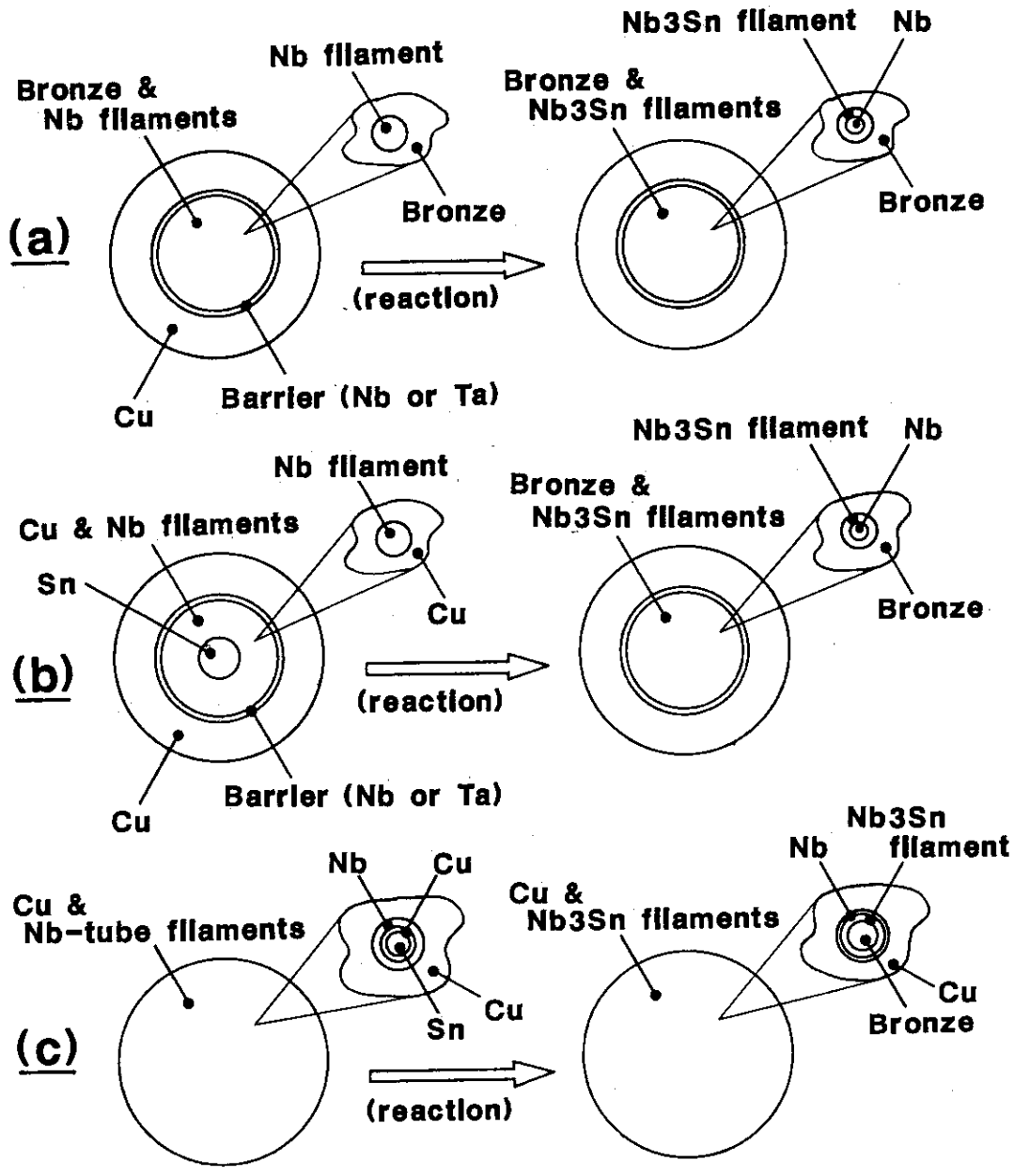

Fig.1 Schematic manufacturing processes of the typical multi-filamentary Nb_3Sn wire.
(a)Bronze process
(b)Internal tin diffusion process
(c)Niobium tube process
(NbTi)3Sn wires are manufactured with the same way except for a few titanium added in somewhere.

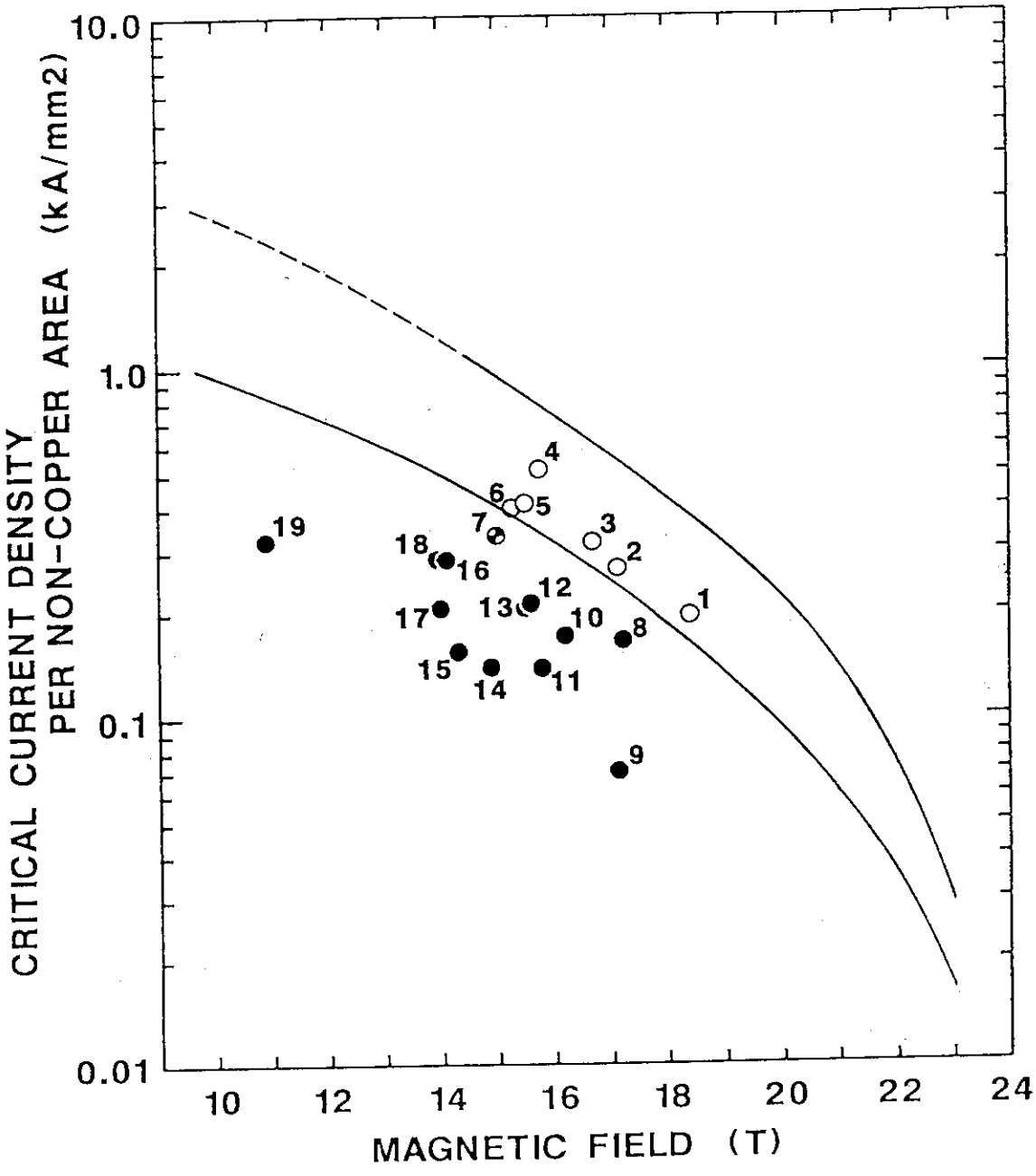

Fig.2 Highest critical current density of the multi-filamentary $(NbTi)_3Sn$ superconductor at 4.2 K manufactured with the bronze process, the internal tin diffusion process and the niobium tube process, which have been published. Circles in this figure are the operating current density of the wires actually in the coils listed in Table 1.

II. Mechanical Properties of the Japanese Cryogenic Steels (JCS) at Cryogenic Temperature

H. Nakajima, K. Yoshida, and H. Tsuji

Superconducting Magnet Laboratory
Division of Thermonuclear Fusion Research
Naka Fusion Research Establishment
Japan Atomic Energy Research Institute

1. INTRODUCTION

Japan Atomic Energy Research Institute (JAERI) started development of new cryogenic steels for the superconducting magnets of the Fusion Experimental Reactor (FER) in collaboration with four steel companies in 1982. JAERI required a strength-toughness combination (σy>1,200 MPa, K_{Ic}>200 MPa$\sqrt{m}$, called JAERI box) that was beyond the capabilities of the existing austenitic stainless steels for cryogenic use. Up to now, JAERI has successfully developed the new cryogenic steels named "Japanese Cryogenic Steels" (JCS). These steels were supplied from industrial heats (5 - 50 tons) and their mechanical properties satisfied requirements mentioned the above. These steels have been already used in superconducting coils, such as JAERI's Demo Poloidal Coils (DPC).

It was already reported that the development of the JCS for the superconducting magnets of the FER.[1] This paper is a summary of mechanical properties of the JCS at cryogenic temperature.

2. REQUIREMENTS FOR THE NEW CRYOGENIC ALLOYS

The conventional austenitic stainless steels, 304L and 316L that were not specially developed for cryogenic use were applied to cryogenic structures. As these steels had poor mechanical properties, nitrogen-strengthened austenitic stainless steels, 304LN and 316LN were substituted for them in

large superconducting coils for LCT program.[2,3] JAERI investigated the effect of carbon and nitrogen contents on the strength and Charpy absorbed energy of 300-series austenitic stainless steels to apply these steels to Japanese LCT coil.[4,5]

However, Structural materials for the superconducting coils of the FER must have higher strength and fracture toughness than 304LN or 316LN at liquid helium temperature. JAERI determined targets for the engineering properties of the structural materials before the specifications of the FER had been fixed.[6,7] The targets which were determined from stress analyses, properties of the superconducting materials, crack propagation analyses, coil operation were as follows:

(1) Yield strength : more than 1,200 MPa at 4 K.
(2) Fracture toughness : more than 200 MPa$\sqrt{m}$ at 4 K.
(Charpy absorbed energy : more than 100 J at 4 K.)
(3) Fatigue characteristics : similar to those of 316 austenitic stainless steel at 4 K.
(4) Magnetic permeability : not specified
(non-magnetic material is preferred).
(5) Corrosion resistance : good rust resistance.
(6) Good workability and weldability.

3. DEVELOPMENT OF THE NEW CRYOGENIC ALLOYS

The data obtained by different laboratories could not be compared because there were no standards for cryogenic material testing. The method of testing at 4 K is very important in evaluating the material properties. Even though the standardization of cryogenic test methods has progressed by a US-Japan collaboration, there still remain several problems.[8,9,10] To eliminate the difficulty of interlaboratory comparisons, it is necessary that only one laboratory conducts material tests at 4 K to select a candidate from the materials produced by different steel companies. Therefore, all tests at 4 K were performed by JAERI. Screening tests to develop new cryogenic steels were tension and Charpy impact tests. Fracture tough-

ness test using computerized unloading compliance technique was conducted for a further screening.[11]

Materials evaluated at JAERI are classified into ferritic steels (FS), high manganese austenitic steels (HMS), austenitic stainless steels (SS), and high manganese austenitic stainless steels (HMSS). Tested steels are all newly developed cryogenic materials except for a few austenitic stainless steel and ferritic steel such as 9% nickel and maraging steel.

Figure 1 shows the relation between the Charpy absorbed energy and the yield strength[12]. Our target shown by the hatched area is located over the line which is extrapolated from 304LN and 316LN austenitic stainless steels. All test results are plotted in this figure. The materials that satisfy the target are austenitic stainless steels and high manganese austenitic stainless steels, except for one ferritic steel and three high manganese austenitic steels. The structural material of the Japanese LCT coil, 304LN manufactured by the electron slag remelting (ESR) process, shows high energy compared with conventional 304LN and 316LN steels. This suggests that the purity of the material affects its toughness. JAERI decided that the austenitic stainless steel development should be continued, and stopped the development of ferritic and high manganese steels. The reason was the poor rust resistance of the latter.

Figure 2 shows the relation between fracture toughness and yield strength. The target, called "JAERI Box", is also located above the trend line for 304-type stainless steels measured by the National Institute of Standards and Technology (formerly National Bureau of Standards)[13]. The results for materials that passed the goals of tension and Charpy tests are plotted in this figure. Half of the tested materials satisfy the target. High Cr-Ni austenitic stainless steels have a better balance of fracture toughness and yield strength in comparison with high Mn austenitic stainless steels.

4. JAPANESE CRYOGENIC STEELS (JCS)

4.1 Mechanical properties of the base metals

From the screening tests, 5 materials were selected and then produced on an industrial scale. These structural alloys were named "Japanese Cryogenic Steels" (JCS). Each name and the corresponding chemical composition is shown in Table 1. All steels are austenitic stainless steels. Two are high Cr-Ni (CSUS-JN1[14,15], JKA1), two are high Mn (CSUS-JN2[15,16,17], JK2[18]), and one is medium chemical composition (CSUS-JJ1[19]). The tensile properties of the JCS are shown in Table 2. The JCS have both high strength and high ductility at 4 K.

Figure 3 shows a typical stress-strain curve for a new cryogenic stainless steel.[20] The stress-strain curve shows a unique and strange behavior, called serration, in the plastic region at 4 K as shown in Fig. 3. The JCS have higher yield strengths than 300-series austenitic stainless steels. But it has lower ductility than that of 300-series austenitic stainless steels. When serrations occur the load drops on the new cryogenic structural materials are larger than those on 304LN austenitic stainless steel as shown in Fig. 3.

Fracture toughness data for the JCS are also shown in Table 2. During fracture toughness tests, serrations occur in the plastic region as observed during the tension tests. Small unstable crack growth, like pop-in cracks, can occur during serrations. However, the JCS materials do not fracture in an unstable fashion. Consequently, the JCS has high fracture toughness.

4.2 Mechanical properties of weldments

The requirements for the mechanical properties of weldments are the same as those for the base metals at cryogenic temperatures. Usually however, weldment properties decrease compared to the base metals. Therefore, we adopted weldments which had the best properties, even if their mechanical properties did not satisfy the target. Tungsten inert gas

(TIG) welding and electron beam (EB) welding were applied to the JCS, and these weldments have been evaluated now[21,22].

The mechanical properties of the weldments are shown in Table 3. The strength of TIG welded joints is lower than that of the base metals. The fracture toughnesses of TIG joints are also lower than those of the base metals. On the other hand, the EBW properties compare favorably with those of the base metals. In fact, the fracture toughnesses of EBW joints of CSUS-JN1, JN2, JK2 are higher than those of the base metals.

4.3 Mechanical properties of Conduit Materials

Thin plates are used for the conduit material of a conductor. The base materials and weldments suffer from cold working when the conductor is formed. In addition, the conduit material for Nb_3Sn conductors suffers from the reaction heat treatment (for example, 700 ℃ x 200 hours), which degrades the ductility of the material due to sensitization. Some verification tests to clarify these problems were conducted before application of the JCS to conduits[23]. Tested materials were CSUS-JN1, JN2, JK2 and JKA1. In addition, specially developed CSUS-JK1[24], whose ductility does not decrease after the Nb_3Sn reaction heat treatment, was tested. The yield and tensile strengths of a thin plate in the solution treated state slightly increased in comparison with those of a thick plate. Both the yield and tensile strengths slightly decreased due to heat treatment. The effect of heat treatment on elongation is a serious problem in some JCS. The elongation of materials subjected to heat treatment drastically degrades, except for that of CSUS-JK1 as shown in Fig. 4. It was verified that CSUS-JK1 was effective for conduits which suffer from Nb_3Sn activation heat treatment, and also that other JCS could be used for the conduits of Nb-Ti conductors.

5. VARIABLES IN CRYOGENIC TESTING

5.1 Effect of specimen size

The effect of specimen size on tensile and fracture toughness properties of the JCS were investigated[25]. Figure 5 shows a load-time chart for a CSUS-JJ1 tension test with a large specimen. The observed tensile behavior is similar to that of the 7 mm diam. specimen. Figure 6 compares the mechanical properties of the 7 mm and 25 mm diam. specimens. Ultimate tensile strength and reduction of area slightly decrease with increased specimen diameter. However, the decreases are equivalent to measurement uncertainties for the material properties.

Figure 7 shows J_{Ic} versus specimen thickness for CSUS-JN1 and JJ1. There is little or no size effect in thick specimens and brittle fracture does not occur even if the plane strain condition is satisfied. However, the fracture toughness of 12.5 mm thick CSUS-JJ1 specimen is higher than those of other thicknesses.

5.2 Effect of Test Rate in Tension Test

Figure 8 shows the yield and ultimate tensile strengths of CSUS-JK2 with varying test rate. Yield strength is not influenced by the test rate, but ultimate tensile strength is decreased at test rates higher than 10^{-3} s^{-1}. Serration phenomena also change with the test rate. Serrations do not occur at high test rates, due to extreme adiabatic heating of the material. With regard to tension test, a consensus method was established under a US-Japan collaboration. This will be standardized as ASTM standard in US [9] and JIS Z 2277 regarding cryogenic tension test was already established based on this consensus method in June 1990 in Japan. The test rate recommended by the standard is less than 10^{-3} s^{-1}. The maximum rates in our tension tests are below that limit.

5.3 Effect of test control in fracture toughness test

Figure 9 shows load-displacement curves of three different controls for 25 mm thick CT specimens. Load-drops during serrations are sharp when displacement control is used. On the other hand, no load-drops and rapid increase of displacement occurs when tests are conducted using load control. Figure 10 shows J - Δa curves for three controls. All data points are on the same curve up to the 0.15 % offset line. But the slope of the regression line using load control is larger than that using other controls, due to different behavior observed in the load-displacement curve when serration occurs. Consequently, the test using load control indicates lower J_{Ic} as compared with stroke or displacement control tests. The JCS, however, did not exhibit brittle fracture even when fracture tests were conducted using load control.

6. APPLICATION OF THE JCS

JAERI used the JCS as structural materials for the Demo Poloidal Coils (DPC)[26,27]. The DPC project aims to develop the technology for the ohmic heating coils of the FER. These coils suffer from complicated cyclic forces due to pulsed operation for plasma ignition. The DPC is composed of three coils; a pair of Nb-Ti forced-flow coils (DPC-U1,U2) and a Nb_3Sn forced-flow coil (DPC-EX), installed between DPC-U1 and DPC-U2. Figure 11 shows a schematic of the DPC. The JCS used in the DPC were thick plates for the coil supports and bolts, and thin plates for the conduit materials and the cryogenic buffer tank. CSUS-JK2 and JK1 were used as coil supports and bolts, respectively. CSUS-JN1 and JK1 were used for the conduit material of the DPC-U1,U2 and DPC-EX, respectively. In addition, CSUS-JKA1 was used for the cryogenic buffer tank.

7. SUMMARY

JAERI, in collaboration with four steel companies, has successfully developed new cryogenic steels, JCS, for the

superconducting magnets of the FER. The new steels have high strength-toughness combinations (σy>1,200 MPa, K_{Ic}>200 MPa$\sqrt{m}$) that are beyond the capability of conventional austenitic stainless steels for cryogenic use, as shown in Fig. 12. These steels have been already used as the structural materials of real superconducting coils, JAERI's Demo Poloidal Coils.

ACKNOWLEDGMENTS

The authors would like to thank Drs T. Iijima and S. Shimamoto for their continuous encouragement of this work. This development was carried out in collaboration with Japan Steel Works Ltd., Kawasaki Steel Corporation, Kobe Steel Ltd., and Nippon Steel Corporation. Without such collaboration, the development of the JCS would not have been possible. The authors wish to express appreciation to all the participants in each industry for their contributions.

REFERENCES

1. H. Nakajima, K. Yoshida, and S. Shimamoto : To be published in ISIJ International, Vol. 30, No.8, (1990), 567
2. S. Shimamoto, T. Ando, T. Hiyama, H. Tsuji, Y. Takahashi, E. Tada, M. Nishi, K. Yoshida, K. Okuno, K. Koizumi, T. Kato, H. Nakajima, O. Takahashi, M. Shimada, Y. Sanada, F. Iida, and K. Yasukochi : IEEE Trans. Magn., MAG-19, (1983), 851
3. S. Shimamoto, T. Ando, T. Hiyama, H. Tsuji, Y. Takahashi, M. Nishi, E. Tada, K. Yoshida, K. Okuno, K. Koizumi, H. Nakajima, T. kato, and K. Yasukochi : Cryogenics, Vol. 25, (1985), 227
4. Y. Takahashi, K. Yoshida, M. Shimada, E. Tada, R. Miura and S. Shimamoto : Adv. Cryog. Eng. Mater., Vol. 28, Plenum Press, New York, (1982), 73
5. R. Miura, K. Ohnishi, H. Nakajima, and S. Shimamoto : Tetsu-to-Hagane, 73, (1987), 715

6. K. Yoshida, H. Nakajima, K. Koizumi, M. Shimada, Y. Sanada, Y. Takahashi, E. Tada, H. Tsuji, and S. Shimamoto : Austenitic Steels at Low Temperature, Plenum Press, New York, (1983), 29
7. H. Nakajima and S. Shimamoto : J. At. Energy Soc. Japan, Vol. 27, (1985), 9
8. H. Nakajima, K. Yoshida, S. Shimamoto, R. L. Tobler, P. T. Purtscher, and R. P. Reed : Adv. Cryog. Eng. Mater., Vol. 34, Plenum Press, New York, (1988), 241
9. H. Nakajima, K. Yoshida, S. Shimamoto, R. L. Tobler, and R. P. Reed : To be published in Adv. Cryog. Eng. Mater., Vol. 36, Plenum Press, New York, (1990), 1069
10. H. Nakajima, K. Yoshida, and S. Shimamoto : Cryogenic Engineering, Vol. 21, (1986), 197
11. H. Nakajima, K. Yoshida, K. Okuno, M. Oshikiri, E. Tada, S. Shimamoto, R. Miura, M. Shimada, S. Tone, K. Suemune, T. Sakamoto, and K. Nohara : Adv. Cryog. Eng. Mater., Vol. 32, Plenum Press, New York, (1986), 347
12. H. Nakajima, K. Yoshida, Y. Takahashi, E. Tada, M. Oshikiri, K. Koizumi, S. Shimamoto, R. Miura, M. Shimada, S. Tone, H. Masumoto, and T. Sakamoto : Adv. Cryog. Eng. Mater., Vol. 30, Plenum Press, New York, (1984), 219
13. R. L. Tobler and R. P. Reed : Materials Studies for Magnetic Fusion Energy Applications at Low Temperatures III, NBSIR 80-1627, National Bureau of Standards, Boulder CO, (1979), 17
14. T. Sakamoto, Y. Nakagawa, I. Yamauchi, T. Zaizen, H. Nakajima, and S. Shimamoto : Adv. Cryog. Eng. Mater., Vol. 30, Plenum Press, New York, (1984), 137
15. K. Suemune, T. Sakamoto, T. Ogawa, T. Okazaki, S. Maehara, H. Nakajima, and S. Shimamoto : Adv. Cryog. Eng. Mater., Vol. 34, Plenum Press, New York, (1988), 123
16. H. Masumoto, K. Suemune, H. Nakajima, and S. Shimamoto : Adv. Cryog. Eng. Mater., Vol. 30, Plenum Press, New York, (1984), 169

17. K. Suemune, K. Sugino, H. Masumoto, H. Nakajima, and S. Shimamoto : Adv. Cryog. Eng. Mater., Vol. 32, Plenum Press, New York, (1986), 51
18. S. Tone, M. Shimada, T. Horiuchi, Y. Kasamatsu, H. Nakajima, and S. Shimamoto : Adv. Cryog. Eng. Mater., Vol. 30, Plenum Press, New York, (1984), 145
19. J. Ishizaka, R. Miura, H. Nakajima, and S. Shimamoto : Tetsu-to-Hagane, Vol 76, No.5, (1990), 149
20. S. Shimamoto, H. Nakajima, K. Yoshida, and E. Tada : Adv. Cryog. Eng. Mater., Vol. 32, Plenum Press, New York, (1986), 23
21. S. Tone, M. Hiromatsu, J. Numata, T. Horiuchi, H. Nakajima, and S. Shimamoto : Adv. Cryog. Eng. Mater., Vol. 32, Plenum Press, New York, (1986), 89
22. T. Ogawa, T. Koseki, S. Ohkita, and H. Nakajima : Welding Journal, No.6, 205s, (1990), 69
23. H. Nakajima, K. Yoshida, M. Oshikiri, Y. Takahashi, K. Koizumi, S. Shimamoto, M. Shimada, S. Tone, S. Sakamoto, K. Suemune, and K. Nohara : Adv. Cryog. Eng. Mater., Vol. 34, Plenum Press, New York, (1988), 173
24. M.Shimada and S. Tone : Adv. Cryog. Eng. Mater., Vol. 34, Plenum Press, New York, (1988), 131
25. K. Yoshida, H. Nakajima, M. Oshikiri, R. L. Tobler, S. Shimamoto, R. Miura, and J. Ishizaka : Adv. Cryog. Eng. Mater., Vol. 34, Plenum Press, New York, (1988), 225
26. H. Tsuji, K. Okuno, H. Nakajima, T. Ando, Y. Takahashi, M. Nishi, K. Yoshida, E. Tada, K. Koizumi, T. Kato, T. Isono, M. Oshikiri, T. Hiyama, K. Kawano, H. Yamamura, M. Sato, J. Yoshida, N. Itoh, and S. Shimamoto : IEEE Trans. Magnetics, Vol. 25, (1989), 1484
27. H. Nakajima, K. Okuno, H. Tsuji, K. Yoshida, K. Koizumi, T. Isono, E. Yaguchi, H. Shimane, and S. Shimamoto : Proc. of 11th International Conference on Magnet Technology, Elsevier Sci. Publ., Ltd., London, (1990), 824

Table 1 Chemical compositions of the JCS

JCS	C	Si	Mn	P	S	Ni	Cr	Mo	N	Others
CSUS-JN1	0.026	0.99	4.2	0.026	0.002	14.74	24.2	--	0.34	
CSUS-JKA1	0.023	0.42	0.49	0.006	0.001	14.0	25.0	0.68	0.268	V:0.30
CSUS-JN2	0.050	0.34	22.4	0.010	0.002	3.22	13.4	0.70	0.24	Cu:0.70
CSUS-JK2	0.05	0.36	21.79	0.013	0.005	4.94	12.82	--	0.212	
CSUS-JJ1	0.046	0.44	9.74	0.020	0.002	11.92	12.21	4.89	0.203	

Table 2 Mechanical properties of the JCS base metals

JCS	YS (MPa)	TS (MPa)	EL (%)	RA (%)	CVN (J)	J_{Ic} (kJ/m^2)	K_{Ic} (MPa$\sqrt{m}$)
CSUS-JN1	1403	1782	40	52	183	196	201
CSUS-JKA1	1295	1534	34	49	250	460	302
CSUS-JN2	1215	1603	36	46	125	182	189
CSUS-JK2	1203	1623	39	52	124	188	202
CSUS-JJ1	1110	1574	43	51	185	372	267

Table 3 Mechanical properties of the JCS weldments

JCS		YS (MPa)	TS (MPa)	J_{Ic} (kJ/m^2)	K_{Ic} (MPa$\sqrt{m}$)
CSUS-JN1	TIG	1196	1553	139	167
	EBW	1396	1761	290	242
CSUS-JKA1	TIG				
	EBW	1293	1602		
CSUS-JN2	TIG	1138	1449	128	157
	EBW	1287	1646	230	216
CSUS-JK2	TIG	1316	1535	125	155
	EBW	1173	1604	269	241
CSUS-JJ1	TIG	1207	1499	197	195
	EBW	1229	1604	307	242

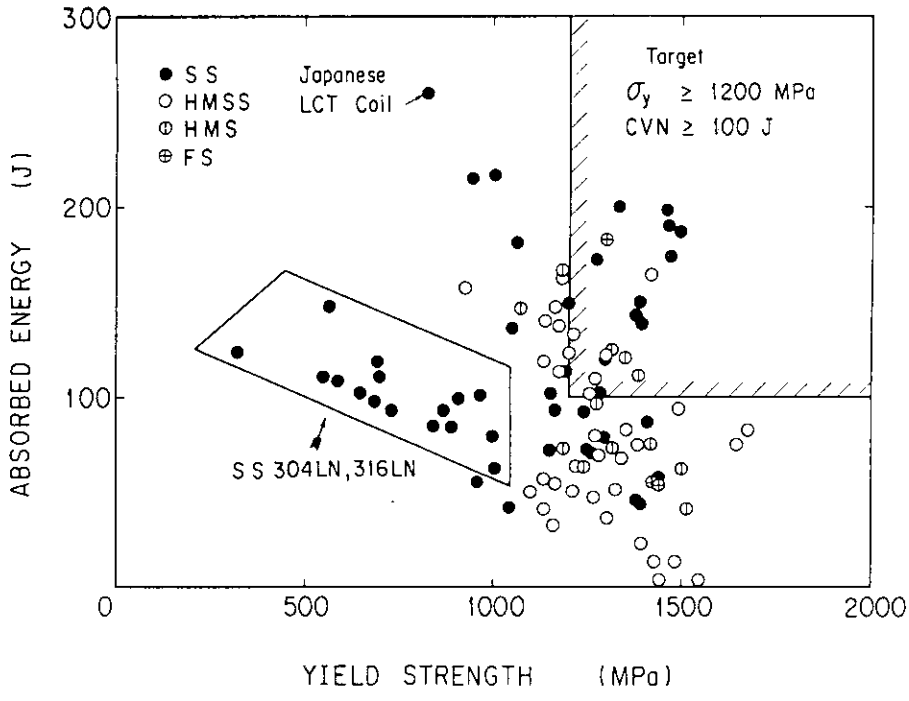

Fig. 1 The relation between the Charpy absorbed energy and the yield strength

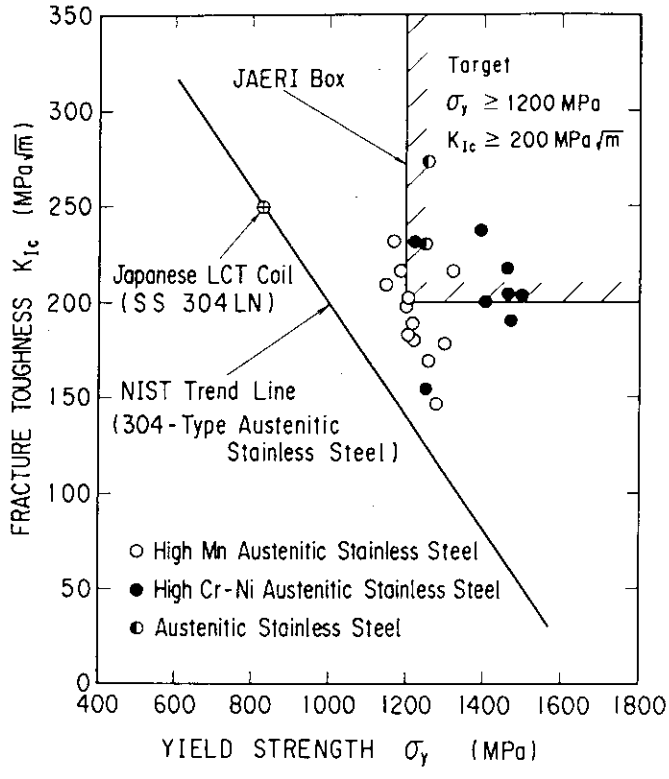

Fig. 2 The relation between fracture toughness and yield strength

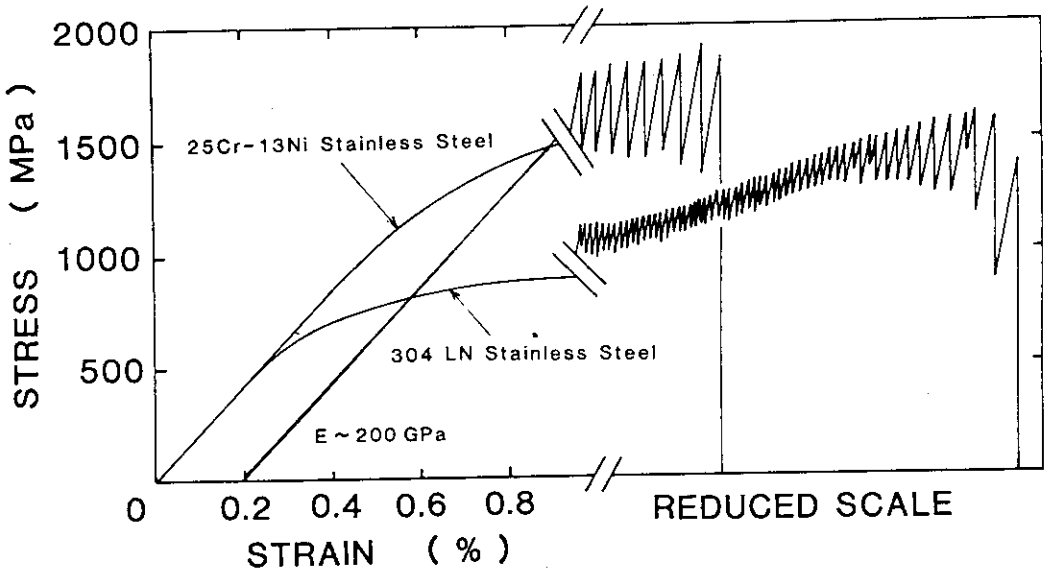

Fig. 3 A typical stress-strain curve for a new cryogenic stainless steel

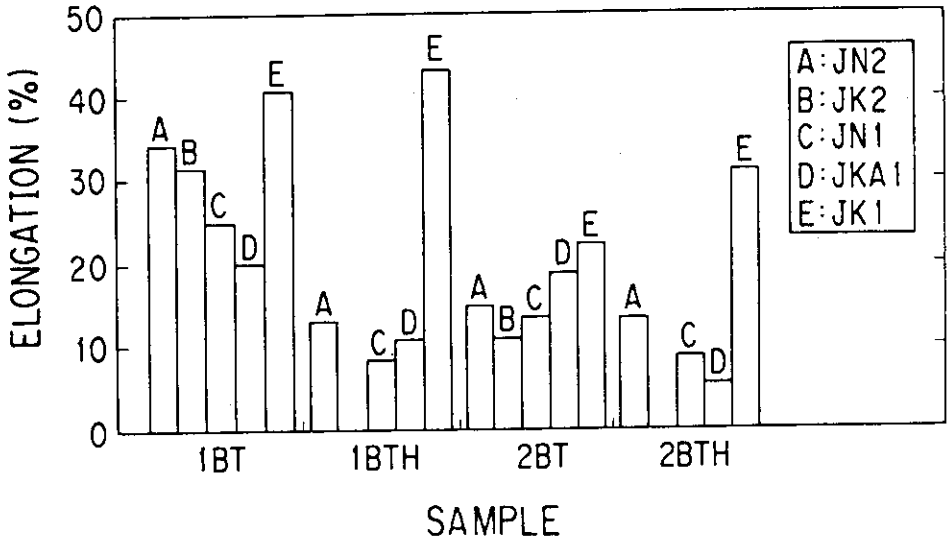

Fig. 4 Elongation of the JCS base metal;

1BT : JCS base metal (ST) in long transverse direction

1BTH : 1BT + 650 - 700 ℃ x 200 h heat treatment

2BT : JCS base metal (ST) + 10 % cold work in long transverse direction + 10 % cold work in longitudinal direction

2BTH : 2BT + 650 - 700 ℃ x 200 h heat treatment

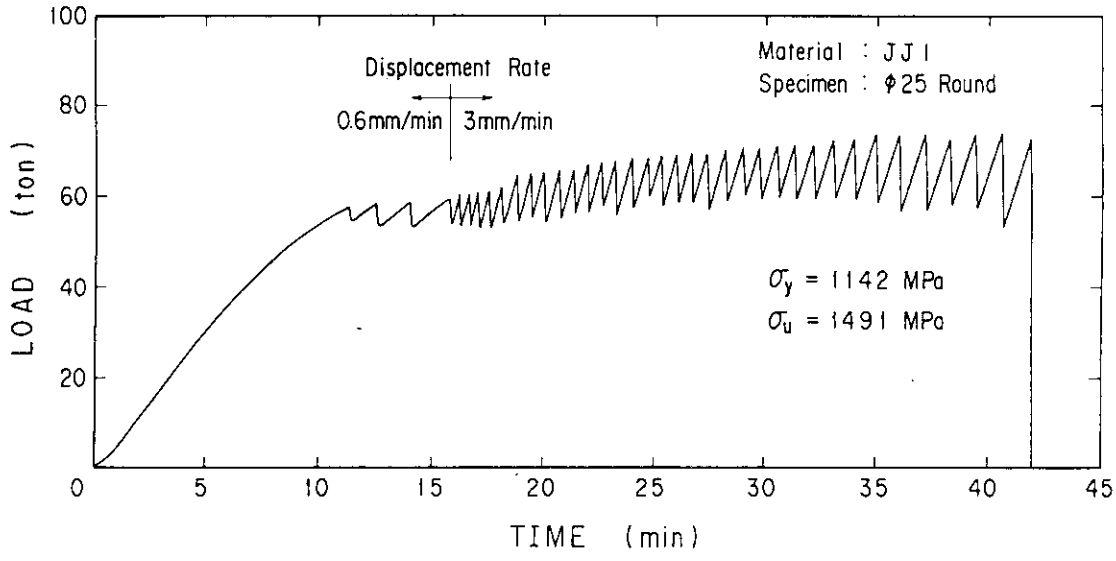

Fig. 5 A load-time chart for a CSUS-JJ1 tension test with a large specimen

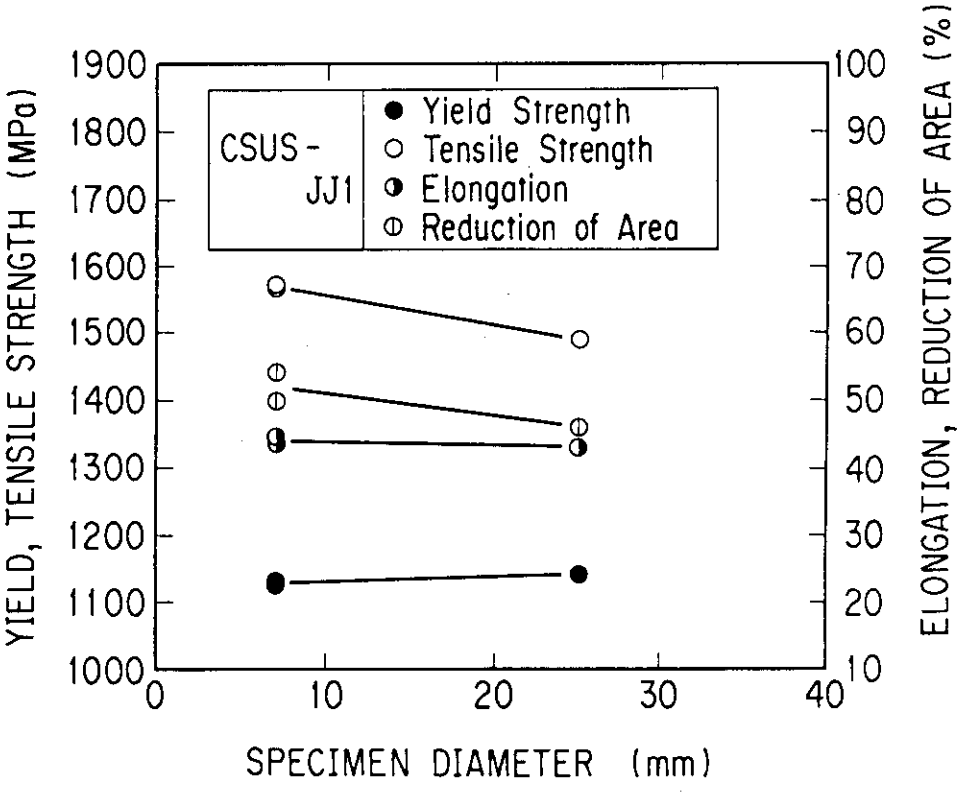

Fig. 6 The tensile properties of the 7 mm and 25 mm diam. specimens

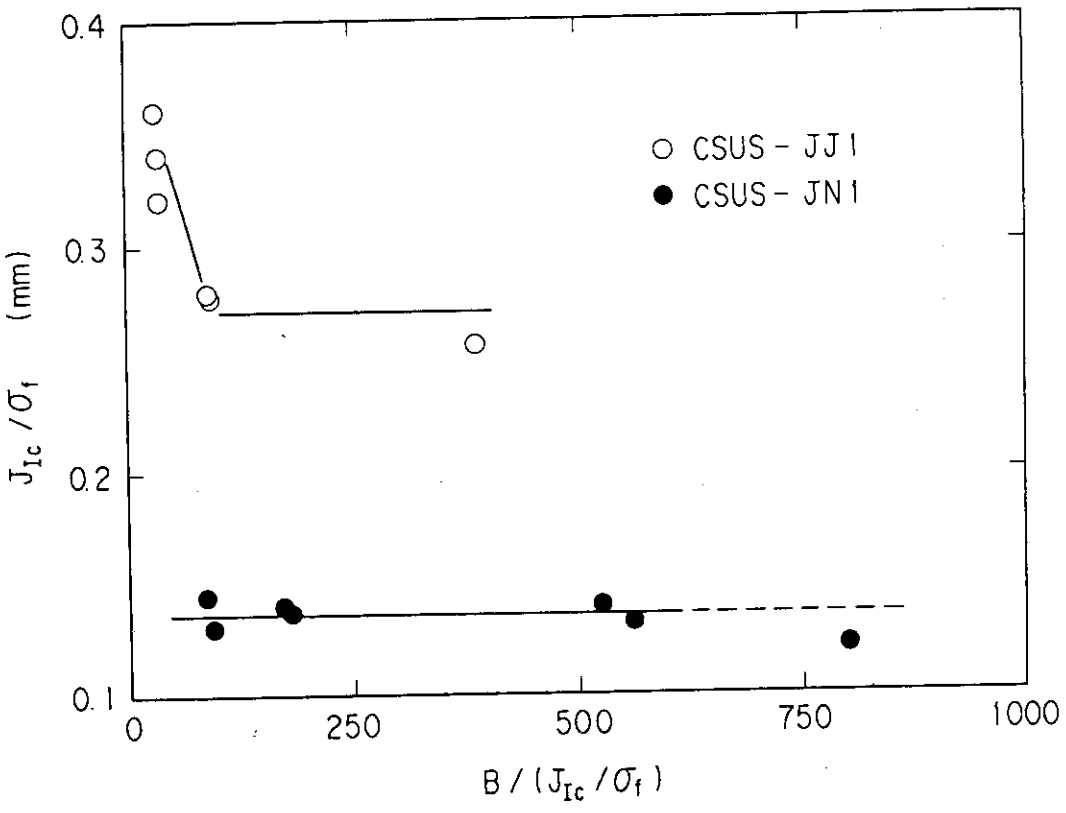

Fig. 7 J_{Ic} versus specimen thickness for CSUS-JN1 and JJ1

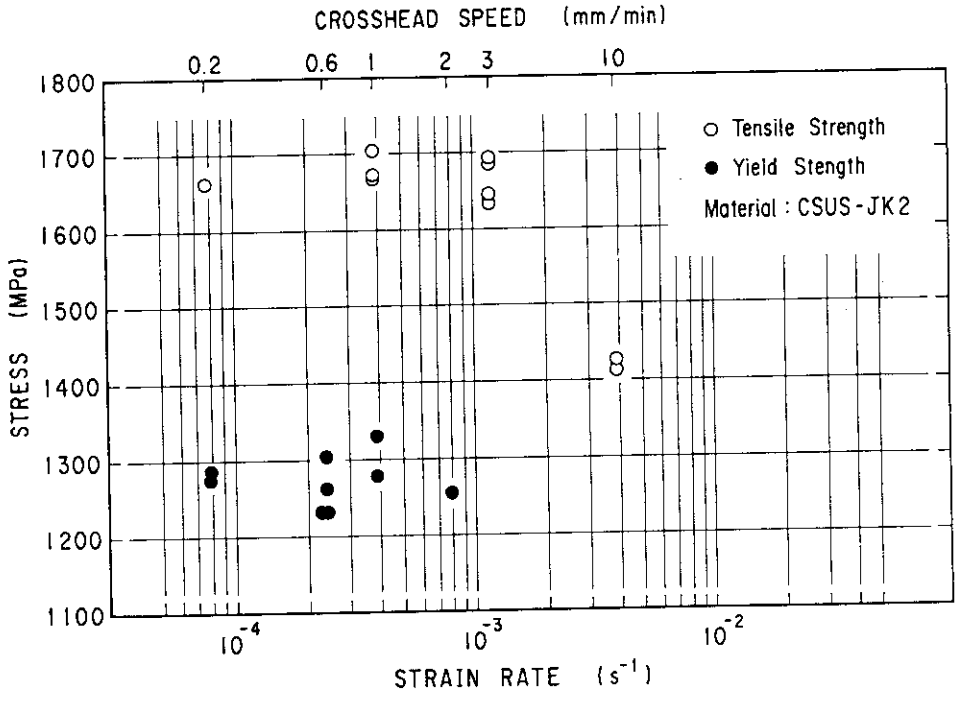

Fig. 8 The yield and ultimate tensile strengths of CSUS-JK2 with varying test rate

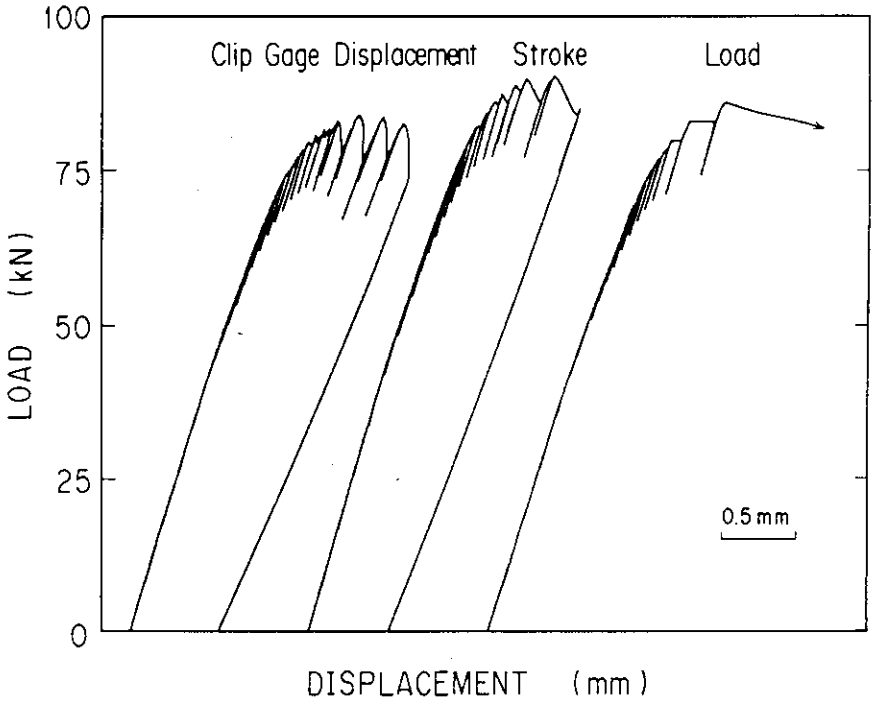

Fig. 9 Load-displacement curves of three different controls for 25 mm thick CT specimens

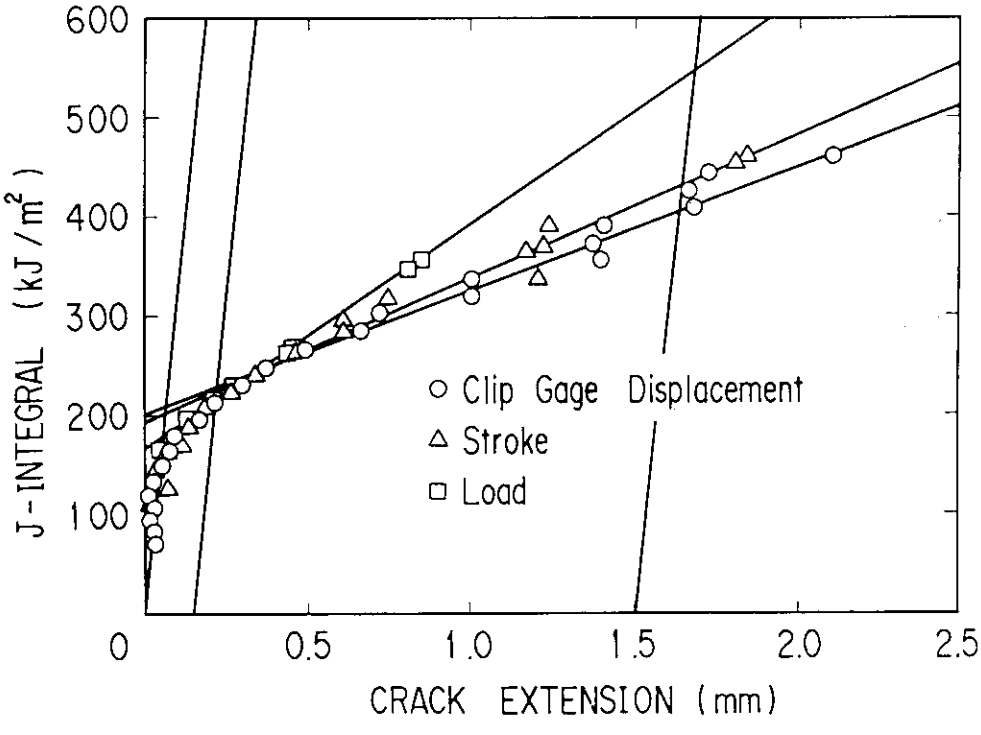

Fig. 10 J - Δa curves for three controls

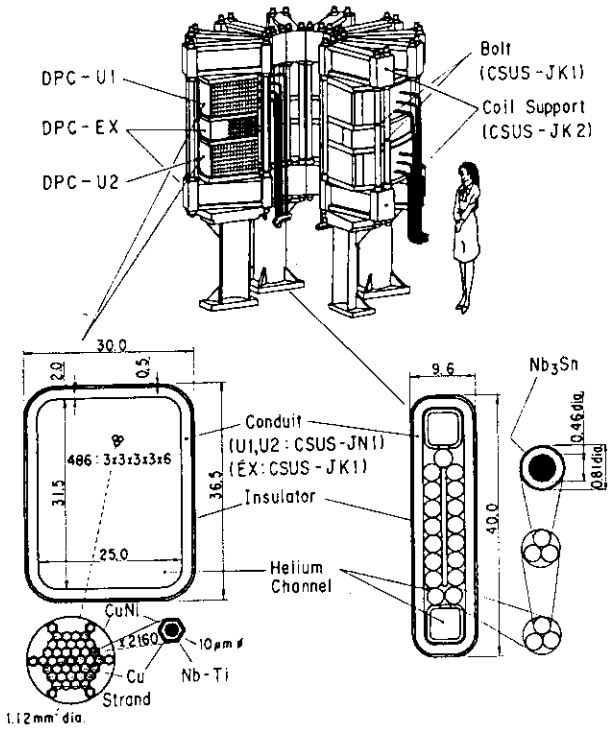

Fig. 11 A schematic of the DPC

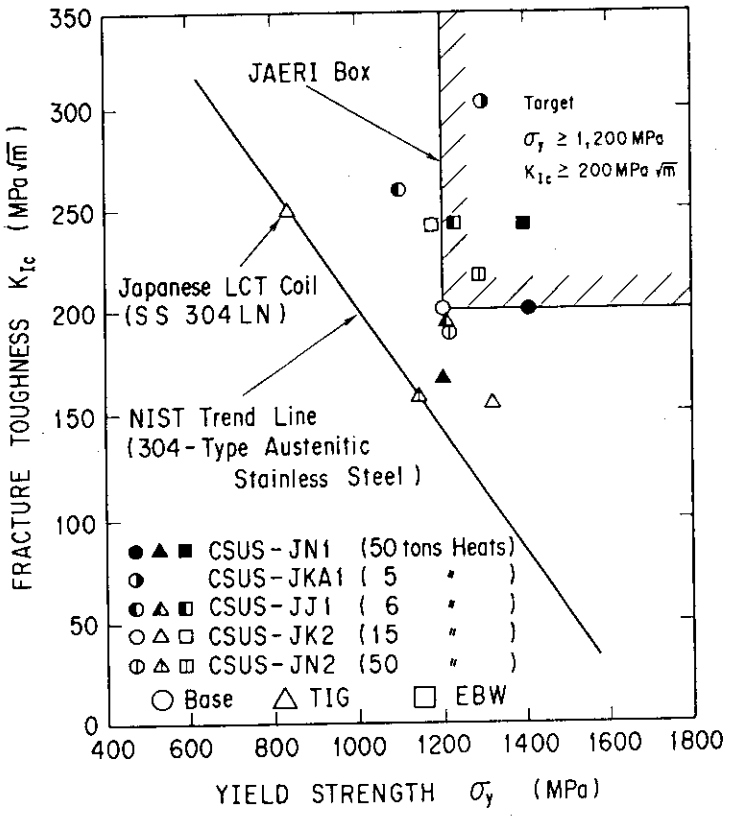

Fig. 12 Mechanical properties of the JCS at 4 K

Ⅲ. Review of Radiation Degradation Studies at JAERI on Composite Organic Insulators Used in Fusion Magnets

S. Egusa,[1] T. Seguchi,[1] M. Hagiwara,[1] H. Nakajima,[2] S. Shimamoto,[2] M. A. Kirk,[3] and R. C. Birtcher[3]

[1]Takasaki Radiation Chemistry Research Establishment, Japan Atomic Energy Research Institute, Takasaki-shi, Gunma 370-12, Japan.

[2]Naka Fusion Research Establishment, Japan Atomic Energy Research Institute, Naka-machi, Naka-gun, Ibaraki 311-02, Japan.

[3]Materials Science and Technology Division, Argonne National Laboratory, Argonne, Illinois 60439, U.S.A.

1. INTRODUCTION

In the construction of superconducting magnets for Tokamak and Mirror type fusion reactors, large amounts of polymer matrix composites are used as mechanical supporters and as electrical and thermal insulators. The magnets will be subjected to substantial quantities of neutrons and γ-rays during the fusion-reactor operation, thus leading to significant degradation of the magnet component materials such as insulators, stabilizers, and superconductors.[1-3] Probably the degradation is most serious for composite organic insulators, because organic materials are usually less radiation resistant than inorganic materials. Thus the operating lifetime of the magnets may be virtually determined by the radiation resistance of the insulators.

The present paper is an interim report on the progress made by the authors since 1983 in understanding the irradiation effects on the mechanical properties of polymer matrix composites to be used in fusion magnets.[4-25] This paper mainly describes the mechanical properties of glass fiber composites tested at 77 K, 4.2 K, and at room temperature after ^{60}Co γ-ray and neutron irradiations at room temperature or at 5 K. Based on the composite degradation behavior, the mechanisms

underlying the irradiation effects on polymer matrix composites are discussed with respect to factors such as composite type, test temperature, radiation type, and irradiation temperature.

2. EXPERIMENTAL

Most composites studied here were especially prepared by using the reinforcing filler shown in Table 1, and the matrix resin of epoxy or polyimide. The epoxy resin was tetraglycidyl diaminodiphenyl methane (TGDDM) cured with diamino diphenyl sulfone (DDS), or diglycidyl ether of bisphenol A (DGEBA) cured with diamino diphenyl methane (DDM). The polyimide resin was polyaminobismaleimide (Kerimid 601). Unless otherwise noted in the text, the matrix resin of TGDDM/DDS epoxy and the E-glass fabric of KS-1210 were used in this work. Commercially available glass fiber composites such as G-10CR and G-11CR were obtained from Spaulding Fibre Company, Inc. The matrix resin in G-10CR was a solid DGEBA cured with dicyanodiamide, while that in G-11CR was a liquid DGEBA cured with DDS. The 1.7-3.2 mm thick sheets of the obtained composites were cut into rectangular specimens of 6.4 mm width and 70 mm length. The cutting was made so that the 70 mm axis was in a 0° or 45° orientation with respect to the warp and fill, thus obtaining 0° or 45° specimens.

^{60}Co γ-ray irradiations were made in air at room temperature with a dose rate of about 0.02 MGy/hr. For some specimens, 2 MeV electrons from a Cockcroft-Walton type accelerator were used in place of γ-rays. The two types of radiation were confirmed to be equivalent in the irradiation effects on polymer matrix composites.[18,25] Neutron irradiations were carried out in the Intense Pulsed Neutron Source (IPNS) at Argonne National Laboratory.[26] The in-air room-temperature irradiations were made in horizontal thimbles called "Rabbit" and "H2", while the 5 K irradiations in liquid helium were made in a vertical thimble called "VT2".

Three-point bend tests were conducted at 77 K, 4.2 K, or at room temperature. For specimens irradiated at 5 K with neutrons, the tests were performed after warmup to room temper-

ature. The failure tests were made at a crosshead speed of 0.5 or 0.6 mm/min with a span length of 20 or 24 mm. The ultimate flexural strength was calculated from $3P_f(\ell/h)/2bh$ for a 0° specimen, while for a 45° specimen the ultimate interlaminar shear strength was calculated from $3P_f/4bh$, where P_f is the applied load at failure, ℓ is the span length, b is the specimen width, and h is the specimen depth (thickness).

3. RESULTS AND DISCUSSION

3.1 Temperature Dependence of Composite Strength

Glass/epoxy composites having various degrees of cure of the matrix resin were prepared by changing the cure conditions.[17] The ultimate flexural strength of a 0° specimen tested at 77 K or at room temperature is plotted in Figure 1 as a function of the glass transition temperature of the matrix resin, T_g. The T_g is closely related to the degree of cure of the matrix resin and its mechanical properties.

The composite strength at room temperature (Fig.1) scarcely depends on the T_g, although in the T_g range below 140 ℃ the strength has a tendency to decrease slightly. This result can be explained by a fiber-controlled failure mode such that the failure of a composite occurs when the composite strain is reached at the ultimate strain of fibers. In this failure mode, the composite strength is independent of the ultimate strain of the matrix as long as the matrix ultimate strain is higher than the fiber ultimate strain. Thus the composite strength at room temperature scarcely depends on the T_g, because usually the matrix resin is more ductile than the fiber.

The composite strength at 77 K (Fig. 1) is lower than that at room temperature in the T_g range below 140 ℃. The strength at 77 K, however, begins to increase with increasing T_g at about 140 ℃, and then levels off at T_g values of 180 ℃ or above, approaching a value about twice that at room temperature. These results can be explained by a matrix-controlled failure mode such that the failure of a composite occurs or at least begins when the composite strain is reached at the matrix ulti-

mate strain. In this failure mode, the composite strength is virtually determined by the matrix ultimate strain instead of the fiber ultimate strain. Thus the composite strength at 77 K depends on the T_g, because the matrix resin becomes brittle on cooling. These considerations lead to a conclusion that when the present glass/epoxy composite is fabricated as a low-temperature material, the T_g value should be used as a monitor for the quality control. In the present work, the glass/epoxy composites having a T_g above 210 ℃ were used as starting material for the study of irradiation effects.

The about two-fold increase in the composite strength on cooling to 77 K in the T_g range above 180 ℃ (Fig. 1) is due, for the most part, to a cooling-induced increase in the bundle strength of E-glass fibers in the composite. In fact, such an increase in the composite strength on cooling occurs also for other kinds of E-glass fiber composites such as the glass/epoxy (DGEBA/DDM), glass/polyimide, G-10CR, and G-11CR composite.[13, 16, 18]

3.2 Degradation Behavior for γ-Ray or Electron Irradiation

The ultimate flexural strength of a 0° specimen tested at 4.2 K is plotted in Figure 2 as a function of the absorbed dose in matrix for the five kinds of E-glass fiber composites irradiated with ^{60}Co γ-rays at room temperature.[12] Comparison of the dose dependence among these composites reveals that the radiation resistance increases in the order of the G-10CR < G-11CR ≒ glass/epoxy (DGEBA/DDM) < glass/epoxy (TGDDM/DDS) < glass/polyimide composites. This result strongly suggests that the radiation resistance of the matrix resin increases in the order of DGEBA type epoxy < TGDDM type epoxy < polyimide, because for all of these composites the reinforcing filler is E-glass fiber cloth with a comparable volume fraction of fibers.

The ultimate flexural strengths of these composites tested at 77 K are essentially the same as those shown in Figure 2 both before and after irradiation.[13] This result appears to be attributed mainly to the temperature dependence of the mechanical properties of the matrix resin. The stiffness of epoxy

resins is, in fact, almost temperature-independent between 4.2 and 77 K, although between 300 and 77 K the stiffness increases by a factor of about 3 on cooling.

The ultimate flexural strength tested at room temperature, on the other hand, differs from that tested at 4.2 or 77 K, as shown in Figure 3 for the glass/epoxy and glass/polyimide composites.[18] Comparison of the 77 K and room-temperature data points for each composite shows that the initial strength at 77 K is about twice that at room temperature, and that a decrease in the strength by irradiation is appreciably greater at 77 K than at room temperature.

The ultimate interlaminar shear strength of a 45° specimen tested at 77 K or at room temperature is plotted as a function of absorbed dose in Figure 4 for the glass/epoxy and glass/polyimide composites.[21] Comparison of the 77 K and room-temperature data points for each composite shows that the initial strength at 77 K is about twice that at room temperature, and that a decrease in the strength by irradiation is appreciably greater at 77 K than at room temperature. It is particularly worth noting that the dose dependence at each temperature follows an identical pattern for the two composites. These findings indicate that the dose dependence of the composite shear strength is dependent only on the test temperature, and is much less dependent on the matrix resin in the composite.

3.3 Degradation Mechanism of Flexural Strength

Figures 2 and 3 show that the dose dependence of the composite flexural strength is quite complicated, depending not only on the matrix resin in the composite but also on the temperature during the mechanical test. As one possibility of the most dominant factor determining such complicated dose dependence, let us consider the ultimate strain of a matrix.

Figure 5 shows a relationship between the composite ultimate strain and the matrix ultimate strain for the 0° specimens of the glass/epoxy and glass/polyimide composites tested at 77 K and at room temperature. The relationship was calculated by using the experimental data for these composites and for the

pure epoxy and polyimide resins irradiated up to the same doses as the composites.[18] The composite ultimate strain is seen to increase with an increase in the matrix ultimate strain in a similar pattern for both of these composites at 77 K. At room temperature, on the other hand, the composite ultimate strain appears to increase at first, and then levels off at a matrix ultimate strain of about 4% or above.

These findings strongly suggest that the polymer matrix composites studied here have at least two different failure modes when tested in the warp direction of the reinforcing fabrics. In Figure 5, the composite ultimate strain which increases linearly with the matrix ultimate strain is most likely assigned to the matrix-controlled failure mode described in the previous section of this paper. The composite ultimate strain which is almost independent of the matrix ultimate strain, on the other hand, is assigned to the fiber-controlled failure mode.

In order to discuss this point quantitatively, we have tried to derive an expression for the relationship between the composite ultimate strain and the matrix ultimate strain.[18] The broken lines in Figure 6 show the matrix- and fiber-controlled failure modes. The solid curve, on the other hand, shows a complex failure mode such that the failure of a composite is caused by interactions between the matrix- and fiber-controlled failure modes. The solid curve indicates that the composite ultimate strain increases with an increase in the matrix ultimate strain at first, and then approaches gradually the fiber ultimate strain. This characteristic of the complex failure mode is, in fact, observed for the composites studied here, as seen in Figure 5. It is reasonably concluded, therefore, that the dose dependence of the composite flexural strength is virtually determined by a change in the matrix ultimate strain due to irradiation.

3.4 Degradation Mechanism of Shear Strength

Figure 4 shows that the glass/epoxy and glass/polyimide composites are quite similar to each other in the dose depend-

ence of the ultimate interlaminar shear strength at each test temperature. The identical dose dependence of the shear strength may reflect a similarity of the fiber/matrix interface between the two composites. The surface treatment of the glass fibers is, in fact, the same for both of these composites. These facts suggest that the degradation of the composite shear strength is dominated by the radiation damage at the fiber/matrix interface rather than that in the matrix.[21]

This idea is consistent with the scanning electron microscope observation reported by Takeda et al. for the same glass/epoxy composite as used in the present work.[11] According to their observation made after interlaminar shear tests, the fracture surface of the irradiated composite displays separation or debonding between the fiber and the matrix, thus reflecting the radiation-induced decomposition of surface-treating compounds at the fiber/matrix interface. It will be reasonable to conclude, therefore, that the degradation of the composite shear strength is virtually determined by a change in the fiber/matrix bond strength due to irradiation.

3.5 Effect of the Type of Reinforcing Fabric

The ultimate flexural strength of a 0° specimen tested at 77 K is plotted as a function of absorbed dose in Figure 7 for the glass/epoxy composites having different reinforcing fabrics shown in Table 1.[25] The plots show that the initial strength of the KS-1210 or WTX-116E fabric composite is 28-40% higher than that of the KS-1600 or WTA-18W fabric composite, thus indicating that the initial strength is dependent on the fabric weave parameters such as the number of fibers in a yarn and the number of yarns in the warp and fill directions. The plots also show that the initial strength is less dependent on whether the reinforcing fiber is E-glass or T-glass.

Following irradiation the strengths of these composites (Fig. 7) decrease monotonically with increasing absorbed dose. Roughly speaking, the dose dependence appears to follow a rather similar pattern for all of these composites, thus suggesting that the degradation of the composite flexural strength

depends neither on the type of fabric weave nor the kind of glass fibers. This result is consistent with the above-mentioned mechanism such that the dose dependence of the composite flexural strength is virtually determined by a change in the matrix ultimate strain due to irradiation.

The fact that the T-glass fiber composites are comparable to the E-glass fiber composites in the radiation resistance (Fig. 7) is of great importance from the standpoint of their applications to fusion magnets. This is because composite insulators in actual fusion magnets are subjected to neutrons and γ-rays simultaneously, with more than half of the total absorbed dose resulting from neutrons. It is now generally recognized that the neutron irradiation of boron-containing E-glass fiber composites produces additional radiation damage due to a $^{10}B(n, \alpha)^{7}Li$ reaction in E-glass fibers, thus significantly decreasing the radiation resistance of the composites towards neutrons.[7,14,15] For boron-free T-glass fiber composites (see Table 1), on the other hand, the extent of the radiation damage due the ^{10}B reaction will be negligible, thus leading to a higher radiation resistance towards neutrons compared to the E-glass fiber composites. These considerations lead to a conclusion that the T-glass fiber composites are more recommendable than the E-glass fiber composites as component materials to be used in fusion magnets.

3.6 Degradation Behavior for Neutron Irradiation

The ultimate flexural strength of a 0° specimen tested at 77 K is plotted in Figure 8 as a function of the total neutron fluence for the glass/epoxy and glass/polyimide composites irradiated in the IPNS thimbles of Rabbit, VT2, and H2.[14,15] Comparison of the degradation behavior between the two composites reveals that the glass/polyimide composite is comparable or even inferior to the glass/epoxy composite in the radiation resistance towards neutrons.

Taking into account the advantages of epoxy resins over polyimide resins in cost and processing, this result is rather unfavorable for the glass/polyimide composite, even though this

composite is superior to the glass/epoxy composites in the radiation resistance towards γ-rays (see Fig. 2 or 3). This is because in actual fusion magnets, the neutron contribution to the total absorbed dose is estimated to be greater than the γ-ray contribution. These considerations lead to a conclusion that the TGDDM/DDS epoxy composite is more recommendable than the polyimide composite as component materials to be used in fusion magnets.

Comparison of the VT2 and Rabbit data points for each composite shown in Figure 8 suggests that the dose dependence of the flexural strength follows an identical pattern regardless of the 5 K and room-temperature irradiations. This finding and the similarity of the neutron spectrum between the VT2 and Rabbit thimbles[26] strongly suggest that the irradiation temperature of 5 K and room temperature has no significant influence on the degradation behavior of a polymer matrix composite.

REFERENCES

1. B.S. Brown, "Radiation Effects in Superconducting Fusion-Magnet Materials," J. Nucl. Mater., **97**, 1-14 (1981).
2. J.L. Scott, F.W. Clinard, Jr. and F.W. Wiffen, "Special Purpose Materials for Fusion Application," J. Nucl. Mater., **133&134**, 156-163 (1985).
3. G.L. Kulcinski, J.M. Dupouy, and S. Ishino, "Key Materials Issues for Near Term Fusion Reactors," J. Nucl. Mater., **141-143**, 3-9 (1986).
4. S. Egusa, M.A. Kirk, R.C. Birtcher, M. Hagiwara, and S. Kawanishi, "Mechanical Properties of Organic Composite Materials Irradiated with 2 MeV Electrons," J. Nucl. Mater., **119**, 146-153 (1983).
5. S. Egusa, M.A. Kirk, R.C. Birtcher, M. Hagiwara, and S. Kawanishi, "Irradiation Effects on the Mechanical Properties of Composite Organic Insulators," Nucl. Instruments Methods in Physics Research, **B1**, 610-616 (1984).
6. A. Udagawa, S. Kawanishi, S. Egusa, and M. Hagiwara, "Radiation Induced Debonding of Matrix-Filler Interface in Or-

ganic Composite Materials," J. Mater. Sci. Lett., **3**, 68-70 (1984).

7. S. Egusa, M.A. Kirk, and R.C. Birtcher, "Neutron Irradiation Effects on the Mechanical Properties of Organic Composite Materials," J. Nucl. Mater., **126**, 152-159 (1984).
8. S. Egusa, M.A. Kirk, R.C. Birtcher, and M. Hagiwara, "Annealing Effects on the Mechanical Properties of Organic Composite Materials Irradiated with γ-Rays," J. Nucl. Mater., **127**, 146-152 (1985).
9. S. Egusa, M.A. Kirk, R.C. Birtcher, and M. Hagiwara, "Neutron and γ-Ray Irradiation Effects in Composite Organic Insulators," J. Nucl. Mater., **133&134**, 795-799 (1985).
10. M. Hagiwara, A. Udagawa, S. Kawanishi, S. Egusa, and N. Takeda, "Degradation Behavior of Fiber Reinforced Composites under Irradiation by 3 MeV Electrons," J. Nucl. Mater., **133&134**, 810-814 (1985).
11. N. Takeda, S. Kawanishi, A. Udagawa, and M. Hagiwara, "Electron Irradiation Effects on Interlaminar Shear Strength of Glass or Carbon Cloth Reinforced Epoxy Composites," J. Mater. Sci., **20**, 3003-3010 (1985).
12. S. Egusa, H. Nakajima, M. Oshikiri, M. Hagiwara, and S. Shimamoto, "Mechanical Strength at 4.2 K of Organic Composite Materials Irradiated with γ-Rays," J. Nucl. Mater., **137**, 173-175 (1986).
13. S. Egusa and M. Hagiwara, "Mechanical Properties of Polymer Matrix Composites at 77 K and at Room Temperature after Irradiation with ^{60}Co γ-Rays," Cryogenics, **26**, 417-422 (1986).
14. S. Egusa, M.A. Kirk, and R.C. Birtcher, "Effects of Neutron Irradiation on Polymer Matrix Composites at 5 K and at Room Temperature. I. Absorbed-Dose Calculation," J. Nucl. Mater., **148**, 43-52 (1987).
15. S. Egusa, M.A. Kirk, and R.C. Birtcher, "Effects of Neutron Irradiation on Polymer Matrix Composites at 5 K and at Room Temperature. II. Degradation of Mechanical Properties," J. Nucl. Mater., **148**, 53-60 (1987).
16. S. Egusa, A. Udagawa, O. Hashimoto, T. Ono, Y. Yamamoto, and K. Sonoda, "Preparation and Radiation-Resistance Evalu-

ation of Glass Fibre Composites Having Various Epoxy Matrices," J. Mater. Sci. Lett., **7**, 503-505 (1988).

17. S. Egusa, T. Seguchi, and K. Sugiuchi, "Relationship between the 77 K Mechanical Properties of Glass/Epoxy Composite and the Glass Transition Temperature of the Matrix Resin," J. Mater. Sci. Lett., **7**, 973-975 (1988).
18. S. Egusa, "Mechanism of Radiation-Induced Degradation in Mechanical Properties of Polymer Matrix Composites," J. Mater. Sci., **23**, 2753-2760 (1988).
19. S. Egusa, "Effect of Radiation on the Mechanical Properties of Polymer Composites," J. Mech. Behavior of Mater., **1**, 1-36 (1988).
20. K. Sonoda, Y. Yamamoto, O. Hashimoto, T. Ono, H. Tomita, A. Udagawa, S. Egusa, T. Sasuga, T. Seguchi, and N. Tamura, "Degradation Behaviour of Fiber Reinforced Plastic under Electron Beam Irradiation," Jpn. J. Appl. Phys., **28**, 1950-1956 (1989).
21. S. Egusa, "Anisotropy of Radiation-Induced Degradation in Mechanical Properties of Fabric-Reinforced Polymer-Matrix Composites," J. Mater. Sci., **25**, 1863-1871 (1990).
22. S. Egusa, "Irradiation Effects and Degradation Mechanism on the Mechanical Properties of Polymer Matrix Composites at Low Temperatures," Advances in Cryogenic Engineering, **36B**, 861-868 (1990).
23. S. Egusa and T. Seguchi, "Polymer Composites as Magnet Materials: Irradiation Effects and Degradation Mechanism of Mechanical Properties," J. Nucl. Mater., in press.
24. S. Egusa, "Effects of Neutrons and γ-Rays on Polymer Matrix Composites as Low-Temperature Materials," Radiat. Phys. Chem., in press.
25. S. Egusa, "Radiation Resistance of Polymer Composites at 77 K: Effects of Reinforcing Fabric Type, Specimen Thickness, Radiation Type, and Irradiation Atmosphere," Cryogenics, in press.
26. R.C. Birtcher, T.H. Blewitt, M.A. Kirk, T.L. Scott, B.S. Brown, and L.R. Greenwood, "Neutron Irradiation Facilities at the Intense Pulsed Neutron Source," J. Nucl. Mater., **108&109**, 3-9 (1982).

Table 1 Plain-Woven Glass Fabrics Used in the Present Work

Reinforcing fabric	Manufacturer	Fiber type	Fiber diameter (μm)	Number of fibers in a yarn	Number of yarns per 25 mm	
					Warp	Fill
KS-1210	Kanebo Ltd.	E-glass[a)]	7	200	53	48
KS-1600	Kanebo Ltd.	E-glass[a)]	9	400	41	32
WTX-116E	Nitto Boseki Co.	T-glass[b)]	7	200	60	58
WTA-18W	Nitto Boseki Co.	T-glass[b)]	9	400	44	34

a) E-glass composition (wt%): SiO_2(55.2), Al_2O_3(14.8), CaO(18.7), MgO(3.3), B_2O_3(7.3), Na_2O+K_2O(0.5), Fe_2O_3(0.3), F_2(0.3), TiO_2(0.1).

b) T-glass composition (wt%): SiO_2(65), Al_2O_3(23), CaO(<0.01), MgO(11), B_2O_3(<0.01), Na_2O+K_2O(<0.1), Fe_2O_3(<0.1), Zr_2O_3(<1.0).

JAERI-M 91-124

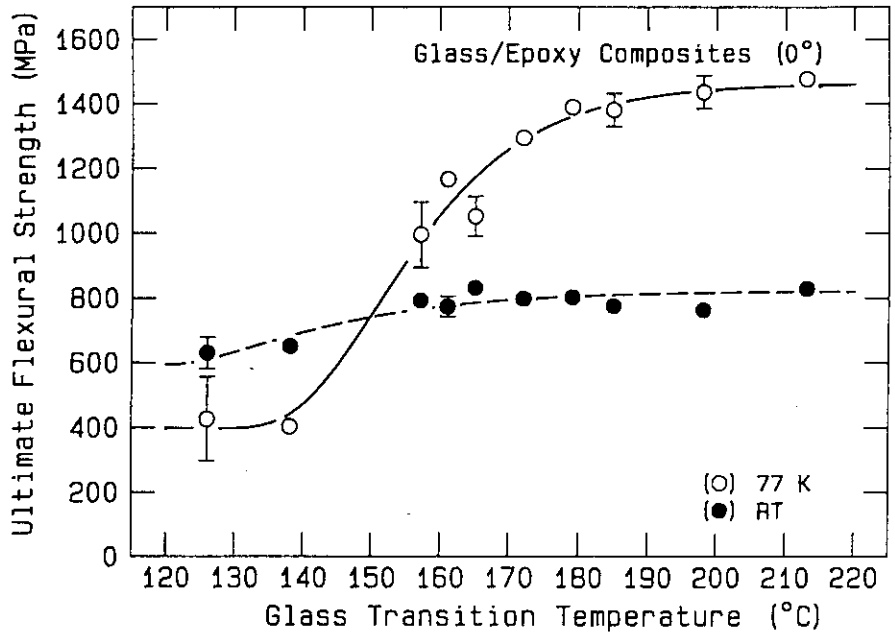

Fig. 1 Plot of the ultimate flexural strength at 77 K and at room temperature versus the glass transition temperature of the matrix resin for the 0° specimens of the glass/epoxy (TGDDM/DDS) composites prepared under the various cure conditions.

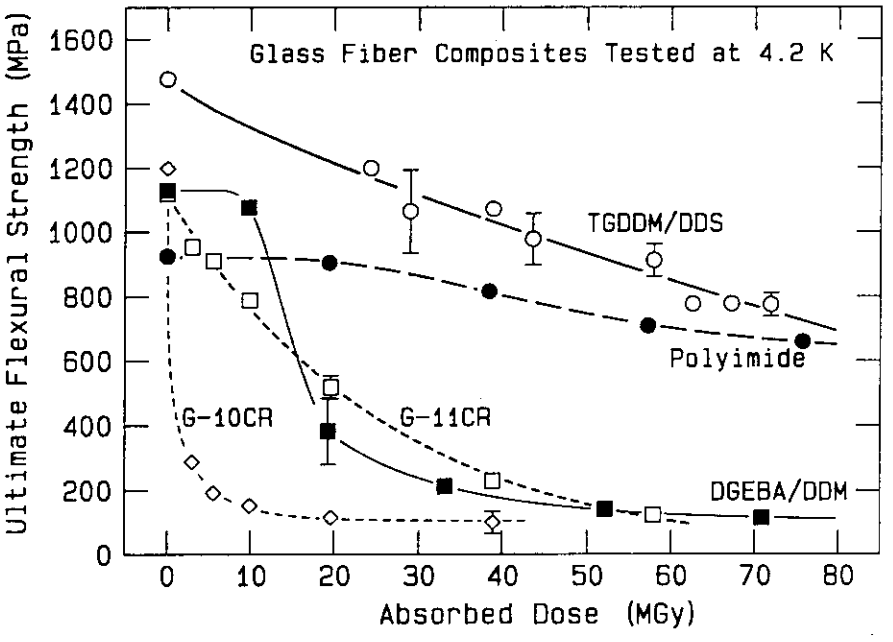

Fig. 2 Plot of the ultimate flexural strength at 4.2 K versus the absorbed dose in matrix for the 0° specimens of E-glass fiber composites irradiated with ^{60}Co γ-rays at room temperature. Only the matrix resin is indicated in this figure to designate the composite, except for G-10CR and G-11CR.

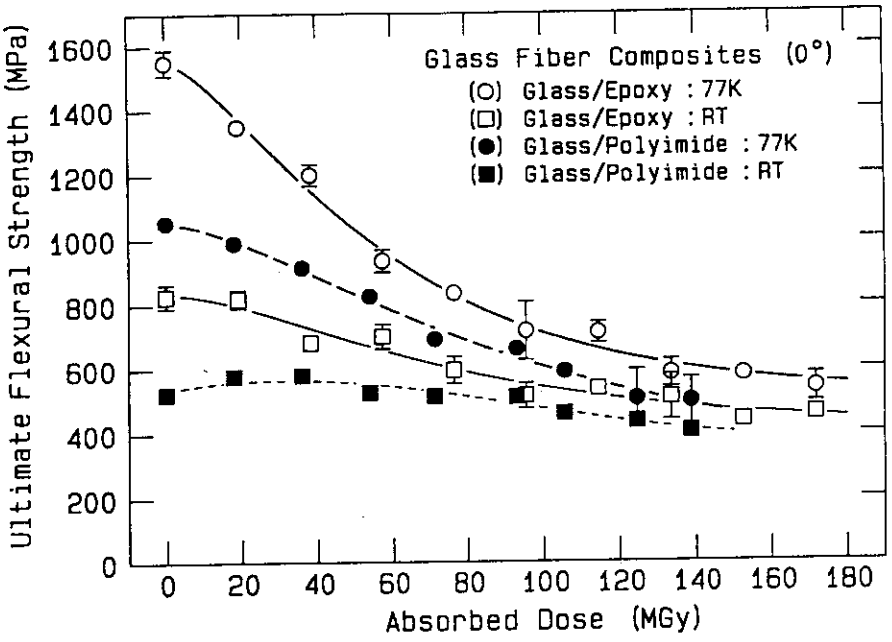

Fig. 3 Plot of the ultimate flexural strength at 77 K and at room temperature versus the absorbed dose in matrix for the 0° specimens of the glass/epoxy (TGDDM/DDS) and glass/polyimide composites.

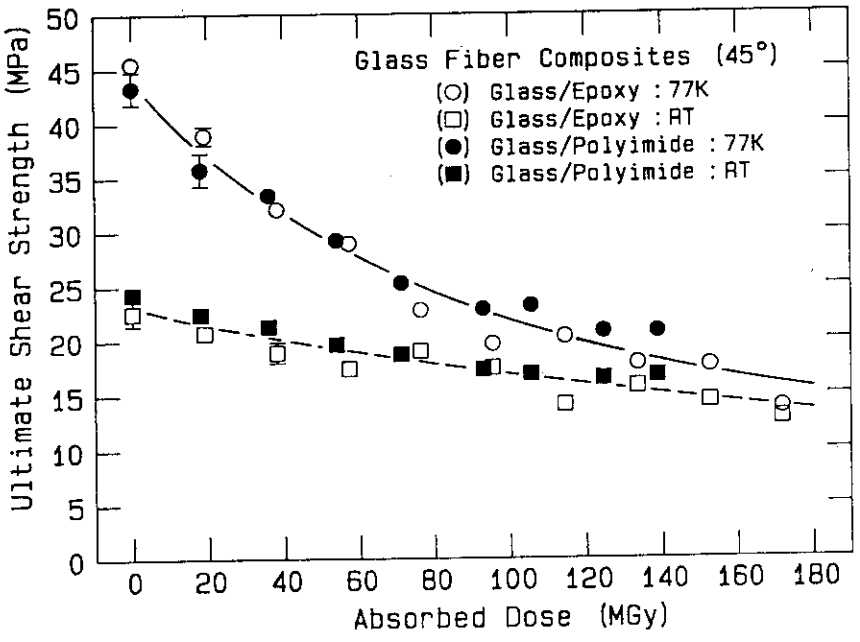

Fig. 4 Plot of the ultimate interlaminar shear strength at 77 K and at room temperature versus the absorbed dose in matrix for the 45° specimens of the glass/epoxy (TGDDM/DDS) and glass/polyimide composites.

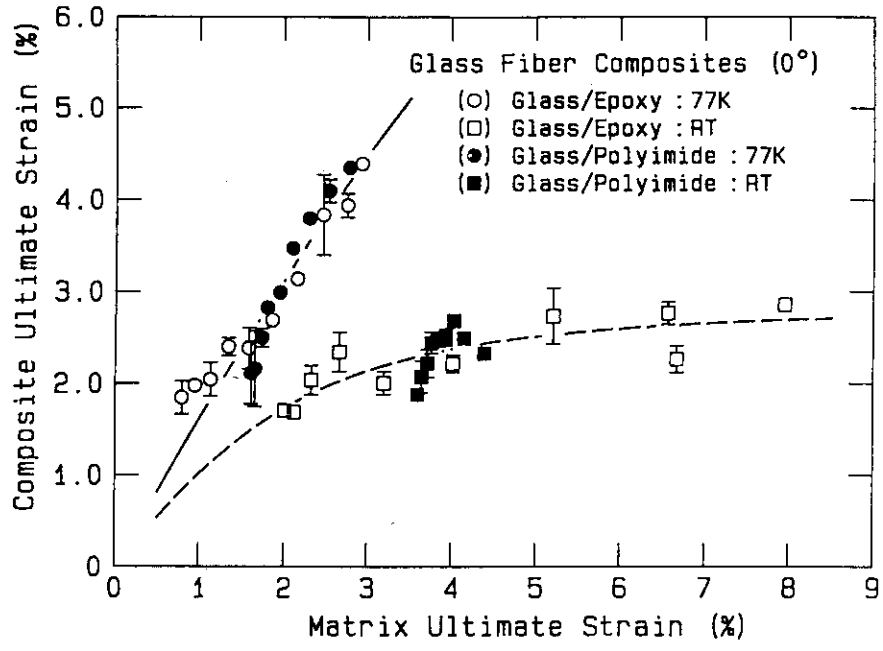

Fig. 5 Relationship between the composite ultimate strain and the matrix ultimate strain for the 0^{o} specimens of the glass/epoxy (TGDDM/DDS) and glass/polyimide composites tested at 77 K and at room temperature.

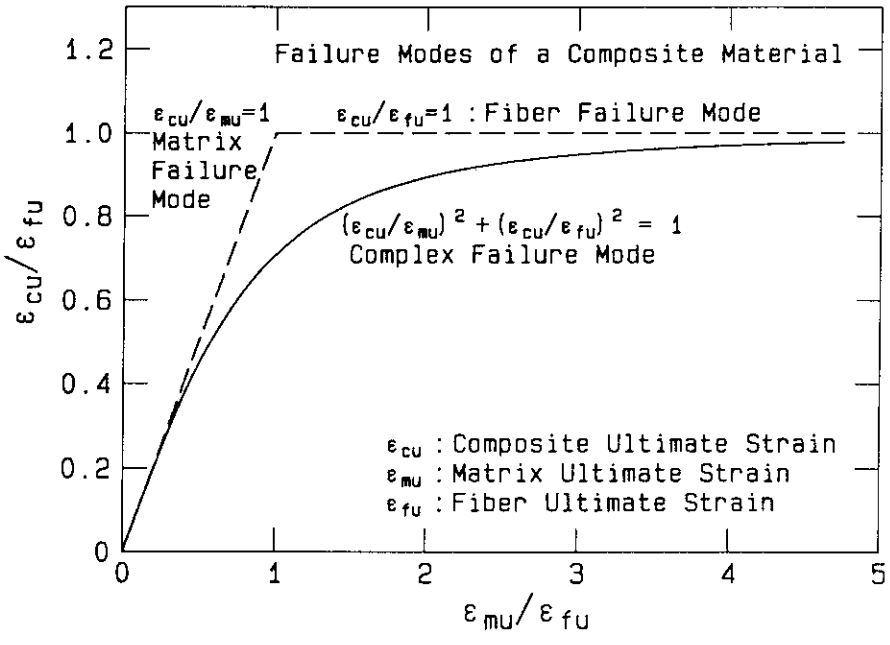

Fig. 6 Modeling of composite failure modes based on a relationship between the composite ultimate strain and the matrix ultimate strain.

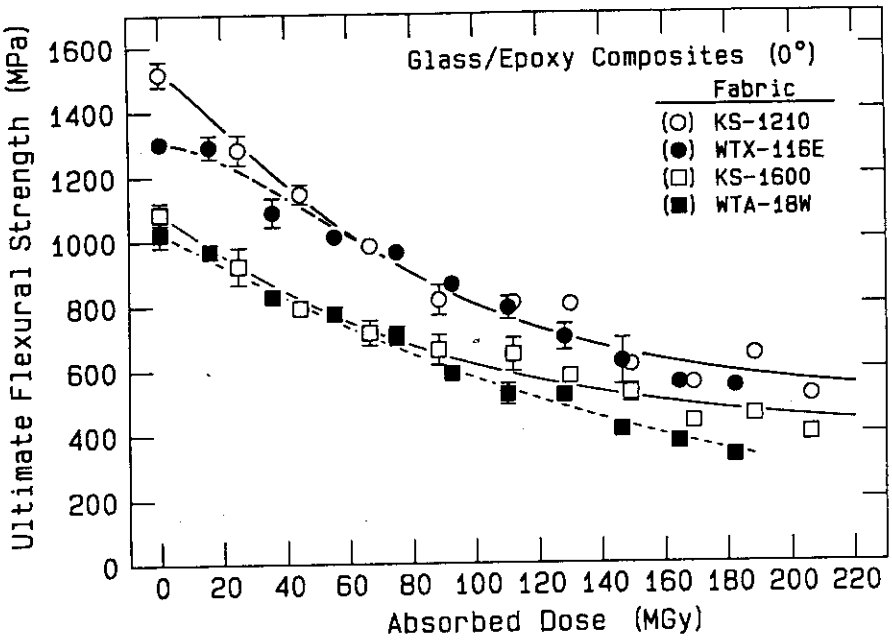

Fig. 7 Plot of the ultimate flexural strength at 77 K versus the absorbed dose in matrix for the 0° specimens of the glass/epoxy composites having different reinforcing fabrics shown in Table I.

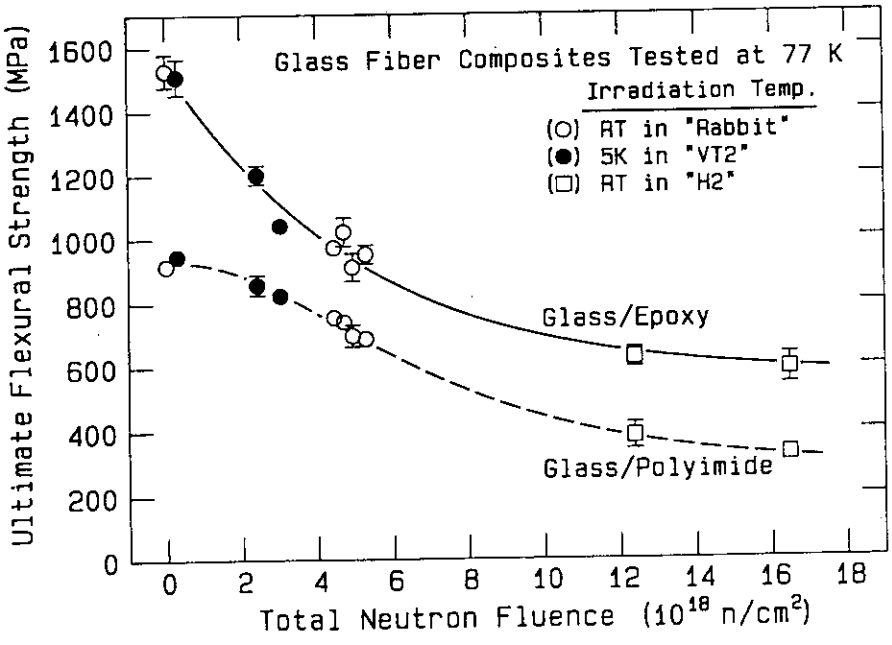

Fig. 8 Plot of the ultimate flexural strength at 77 K versus the total neutron fluence for the 0° specimens of the glass/epoxy (TGDDM/DDS) and glass/polyimide composites irradiated in the IPNS thimbles of Rabbit, VT2, and H2.